European **J**ournal of **Chem**istry

Effects of solvents on the aromaticity and thermodynamic properties of azacalix[2]arene[2]pyrimidines: A computational study

Alihan Tosun [iD] and Fatma Kandemirli [iD] *

Department of Biomedical Engineering, Faculty of Engineering and Architecture, University of Kastamonu, Kastamonu, 37150, Turkey

* Corresponding author at: Department of Biomedical Engineering, Faculty of Engineering and Architecture, University of Kastamonu, Kastamonu, 37150, Turkey.
 e-mail: *fkandemirli@yahoo.com* (F. Kandemirli).

ABSTRACT

The Harmonic Oscillator Model of Aromaticity (HOMA) indexes for the 2,4,6,8-tetraaza-1(2,4),5(4,2)-dipyrimidina-3,7(1,3)-dibenzenacyclooctaphane (TPB) molecule were calculated in gas, ethanol, *n*-octanol and water phase. Solvent effects were analyzed with the use of the Integral Equation Formalism Polarizable Continuum Model (IEFPCM) as the default in the self-consistent reaction field (SCRF) method in Gaussian09. The HOMA indexes indicate the presence of highly aromatic pyrimidine and benzyl rings while the parameters for pyrimidine rings slightly decrease and those for the benzyl ring slightly increase with increasing dielectric constant. According to the results, the pyrimidine ring shows the highest aromaticity in the gas phase and a slight decrease in more polar solvents. In contrast, the benzene ring shows an increase in aromaticity as the solvent polarity increases. The HOMO energy of the TPB shifts downward in more polar solvents and the most significant shift occurs in the water phase. The HOMO-LUMO energy gap increases in polar solvents, indicating higher chemical stability and decreased reactivity in these solvents. These findings provide insight into the stability and reactivity of TPB in different phases for potential applications. In addition, apparent thermodynamic properties such as the heat capacity, entropy, enthalpy, and Gibbs free energy of TBP in various solvents were calculated. Using computational simulations, we derive heat capacity equations that exhibit similar quadratic and linear terms in both phases, differing only in their constants. The negative quadratic term leads to a decrease in heat capacity at very low temperatures.

1. Introduction

Pyrimidine, a class of heterocyclic compounds, has wide applications in pharmaceutical research due to its wide range of biological effects such as anticancer [1,2], anti-inflammatory, analgesic, anthelmintic [3,4], and antimicrobial activity [5]. Among its derivatives, 2,4-diaminopyrimidines have attracted attention due to their highly effective therapeutic properties against cancer and their favorable pharmaceutical properties [6,7]. They synthesized a series of novel azacalix[2]arene[2]pyrimidines and evaluated their antiproliferative activities against human cancer cell lines A549, MCF7, SH-SY5Y, and CNE *in vitro* using the CCK-8 assay [8].

Cancer continues to be one of the most complex and deadly health problems in human history [9]. According to the World Health Organization (WHO), the disease claimed the lives of approximately 8.8 million people in 2015, making it the second most common cause of death worldwide after cardiovascular diseases. The global burden of cancer is particularly pronounced in low- and middle-income countries due to inadequate health infrastructure and limited resources. WHO projections predict that cancer-related deaths will reach 15 million annually by 2030, highlighting the need to develop innovative, effective treatment approaches in the fight against cancer [10]. The biological nature of cancer makes its diagnosis and treatment highly complex. The heterogeneous nature of cancer at the molecular level is influenced by genetic mutations, epigenetic changes, and disturbances in cellular communication pathways, which accelerate tumor formation and progression. In particular, metastatic cancer types and chemotherapy-resistant tumors are seen as one of the biggest challenges that limit the effectiveness of current treatment modalities. In this context, a better understanding of the basic mechanisms of cancer biology is critical for the development of more targeted and effective therapeutic approaches to combat this disease [11]. Therefore, understanding the molecular behavior of pyrimidine derivatives under different conditions is of great importance for the development of more effective drugs.

Despite the stated biological importance of these compounds, the effects of environmental factors such as solvent polarity on their stability and electronic properties have not yet been sufficiently investigated. Computational methods, especially Density Functional Theory (DFT) [12] with the B3LYP functional, provide valuable information on molecular behavior with relatively low computational costs [13].

Table 1. HOMA index of TPB *.

HOMA	A	B	C	D
Gas	0.967879	0.967392	0.967881	0.967392
n-Octanol	0.963554	0.967521	0.963554	0.967523
Ethanol	0.962927	0.968110	0.962928	0.968109
Water	0.962698	0.968300	0.962698	0.968300

* A and C pyrimidine groups, and B and D phenyl groups.
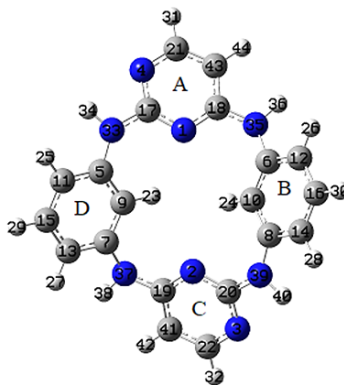
Figure 1. Optimized form with the number of atoms for the 2,4,6,8-tetraaza-1(2,4),5(4,2)-dipyrimidina-3,7(1,3)-dibenzenacyclooctaphane.

The Gaussian 09W [14] and GaussView [15] software facilitates input generation and output analysis for such studies. The IEFPCM model [16] is a continuum solvation model that simulates solvent effects by treating the solvent as a dielectric medium and offers advantages in predicting energy levels, molecular stability, and reactive site analysis in polar and nonpolar media [17,18].

The current study aims to investigate the effect of different solvents, including *n*-octanol, ethanol, and water, on the stability order of the 2,4,6,8-tetraaza-1(2,4),5(4,2)-dipyrimidina-3,7(1,3)-dibenzenacyclooctaphane (TPB) molecule. The stability results obtained in each solvent are compared with each other and with those of the gas phase. Furthermore, molecular orbital (MO) energies are analyzed to examine the role of charge transfer in the stability of the studied complex across different solvents. Furthermore, molecular electrostatic potential (MEP) analysis, frontier molecular orbitals (FMO), and thermodynamic parameters of TPB are studied using the B3LYP method with the 6-311G(d,p) basis set in gas, *n*-octanol, ethanol and water phases. Moreover, the thermodynamic properties, including enthalpy, entropy, and specific heat, are investigated with respect to temperature changes to provide deeper insight into the thermal behavior of TPB in various solvents. This comprehensive investigation provides insights into how the solvent polarity influences the electronic structure and stability of the TPB molecule. The findings could enhance the understanding of solvent effects on similar macrocyclic compounds and their potential applications in various fields, such as supramolecular chemistry.

2. Experimental

For all calculations, we used Density Functional Theory (DFT) [12] at B3LYP [13] theory level. The structure of the 2, 4, 6, 8-tetraaza-1(2, 4), 5(4, 2)-dipyrimidina-3, 7(1, 3)-dibenzena cyclooctaphane (TPB) molecule was fully optimized in both the gas phase and solvent phases, including *n*-octanol, ethanol, and water using B3LYP hybrid density functional, which includes the nonlocal exchange term with three parameters of Becke and the correlation term of Lee-Yang-Parr [13,19] and 6-311G(d,p) basis set.

The IEFPCM [16] model was used to analyze HOMA, LUMO, the aromaticity index, and the thermodynamic parameters in specified solvents. The dielectric constant of the gas phase is 1.

The solvents used in our calculations are *n*-octanol, ethanol, and water with dielectric constants of 9.8629, 24.852 and 78.355, respectively. The dielectric constant order of solvents is gas < *n*-octanol < ethanol < water.

The optimized structures were then used for the determination of thermodynamic parameters, and investigation of properties such as HOMO, LUMO. Contributions of atomic orbitals to HOMO and LUMO in both the gas phase and the solvent phases, including n-octanol, ethanol, and water- were calculated using the Multiwfn program [20]. The surface properties of TPB were analyzed using Multiwfn in the gas phase and in solvent phases such as *n*-octanol, ethanol, and water, using the B3LYP method and the 6-311G(d,p) basis set. The surface properties and HOMA indices of TPB in the gas phase and the solvent phase were carried out using data obtained from B3LYP and 6-311g(d,p) with the Multiwfn program [21].

3. Results and Discussion

The optimized form of the TPB structure, including atomic numbering, is shown in Figure 1. There are two pyrimidine rings labeled A and C and two benzyl groups labeled B and D. The HOMA values of the A ring and C are nearly identical.

The HOMA values of the A ring (pyrimidine group) for gas, *n*-octanol, ethanol, and water phases are 0.967879, 0.963554, 0.962927, 0.962698, respectively, supporting that the interactions can slightly affect the HOMA index (Table 1), but the changes are minimal due to the highly aromatic nature of the pyrimidine group [22]. The decrease in aromacity of the pyrimidine ring of TPB is 0.45, 0.51, and 0.54% as we move from the gas phase to octanol, ethanol, and finally water, which means that the aromaticity of the pyrimidine ring is highest in the gas phase and decreases progressively as the solvent polarity increases. On the contrary, the increase in aromacity of the benzene ring of TPB is 0.013, 0.074, and 0.093% as we move from the gas phase to octanol, ethanol, and finally water shows that the aromaticity of the benzene ring is the highest in the water phase and increases progressively as the solvent polarity increases.

The HOMA index for group B (benzyl) is 0.967392, which is lower than that of the pyrimidine group of TPB due to the electron-withdrawing effect of nitrogen atoms [22].

Table 2. Contribution to HOMA for TPB.

Group	Bonds	Gas	*n*-Octanol	Ethanol	Water
A	17C-4N	-0.002263	-0.002092	-0.001983	-0.001929
	4N-21C	-0.000007	-0.000240	-0.000334	-0.000384
	21C-43C	-0.004044	-0.005548	-0.005752	-0.005844
	43C-18C	-0.025113	-0.027514	-0.027878	-0.027975
	18C-1N	-0.000156	-0.000388	-0.000432	-0.000463
	1N-17C	-0.000538	-0.000664	-0.000692	-0.000708
B	10C-6C	-0.003700	-0.004381	-0.004301	-0.004280
	6C-12C	-0.006749	-0.006447	-0.006260	-0.006196
	12C-16C	-0.000007	-0.000154	-0.000221	-0.000254
	16C-14C	-0.000586	-0.000169	-0.000107	-0.000080
	14C-8C	-0.013939	-0.013406	-0.013155	-0.013029
	8C-10C	-0.007627	-0.007922	-0.007845	-0.007861
C	41C-19C	-0.025112	-0.027514	-0.027878	-0.027975
	19C-2N	-0.000156	-0.000388	-0.000432	-0.000463
	2N-20C	-0.000538	-0.000664	-0.000692	-0.000707
	20C-3N	-0.002263	-0.002092	-0.001984	-0.001929
	3N-22C	-0.000007	-0.000240	-0.000334	-0.000384
	22C-41C	-0.004300	-0.005548	-0.005752	-0.005844
D	15C-11C	-0.000586	-0.000168	-0.000107	-0.000080
	11C-5C	-0.013940	-0.013406	-0.013155	-0.013027
	5C-9C	-0.007626	-0.007920	-0.007847	-0.007863
	9C-7C	-0.003701	-0.004380	-0.004301	-0.004281
	7C-13C	-0.006748	-0.006448	-0.006260	-0.006195
	13C-15C	-0.000007	-0.000154	-0.000221	-0.000254

Table 3. Bond length (Å) of the TPB ring.

A	Gas	*n*-Octanol	Ethanol	Water
17C-4N	1.346048	1.345280	1.345586	1.345125
4N-21C	1.333328	1.338632	1.337920	1.338964
21C-43C	1.378296	1.376427	1.376634	1.376336
43C-18C	1.412180	1.413477	1.413310	1.413521
18C-1N	1.337163	1.339266	1.338991	1.339449
1N-17C	1.339876	1.340662	1.340525	1.340739
B	**Gas**	***n*-Octanol**	**Ethanol**	**Water**
10C-6C	1.397282	1.398007	1.398100	1.397982
6C-12C	1.400536	1.400252	1.400011	
12C-16C	1.388405	1.390269	1.389896	1.390433
16C-14C	1.384306	1.386422	1.386019	1.386632
14C-8C	1.406015	1.405501	1.405667	1.405417
8C-10C	1.401326	1.401515	1.401581	1.401528
C	**Gas**	***n*-Octanol**	**Ethanol**	**Water**
41C-19C	1.412180	1.413477	1.413310	1.413521
19C-2N	1.337163	1.339266	1.338991	1.339449
2N-20C	1.339876	1.340661	1.340526	1.340737
20C-3N	1.346048	1.345281	1.345585	1.345124
3N-22C	1.333328	1.338632	1.337920	1.338966
22C-41C	1.378297	1.376427	1.376634	1.376335
D	**Gas**	***n*-Octanol**	**Ethanol**	**Water**
15C-11C	1.384306	1.386422	1.386020	1.386632
11C-5C	1.406016	1.405501	1.405668	1.405416
5C-9C	1.401325	1.401516	1.401579	1.401531
9C-7C	1.397283	1.398007	1.398099	1.397983
7C-13C	1.400535	1.400073	1.400252	1.400010
13C-15C	1.388405	1.390268	1.389896	1.390432

The HOMO values of the B ring for the gas, *n*-octanol, ethanol, and water phase are 0.967392, 0.967521, 0.968110, and 0.968300, respectively, indicating that the solvent interactions slightly affect the HOMA index, but the changes are minimal due to the highly aromatic nature of the pyrimidine group [23]. The increase in aromaticity of the pyrimidine ring for TPB is 0.013, 0.07 and 0.09%, respectively (Table 2).

17C-4N deviates slightly from the ideal bond length, leading to a slightly negative contribution to HOMA, in other words, slightly broken aromaticity for the pyrimidine group [24]. The 17C-4N bond lengths for gas, *n*-octanol, ethanol, and water phase are 1.346048, 1.345280, 1.345586, and 1.345125 Å. The negative contribution decreases from the gas phase to the liquid phase for the pyrimidine group of TPB. The decreasing order is the gas phase (-0.002263) > *n*-octanol (-0.001983) > ethanol (-0.002092) > water (-0.001929). In contrast, the negative contribution increases for the 10C-6C bond from the gas phase to the liquid phase for the benzyl group of TPB, and the increasing order is the gas phase (-0.003700) < n-octanol (0.00438) > ethanol (-0.004301) > water (-0.004280) and the corresponding length of the 10C-6C bond in the gas, n-octanol, ethanol, and water phase are 1.397282, 1.398007, 1.398100, 1.397982 Å, respectively (Table 3).

The ideal bond length of a C-C bond in an aromatic system is generally accepted as 1.388 Å. A significant deviation from this value indicates a disturbance in aromaticity. The bond lengths of specific C-C pairs of 10C-6C, 6C-12C, 12C-16C, 16C-14C, 14C-8C, and 8C-10C - are measured as 1.397282 Å, 1.400536 Å, 1.388405 Å, 1.384306 Å, 1.406015 Å, and 1.401326 Å, respectively. Among these, the bond length of 14C-8C (1.406015 Å) deviates significantly, leading to a notable negative contribution to the Harmonic Oscillator Model of Aromaticity (HOMA). Specifically, in the gas phase, this bond contributes -0.013939 to the disruption of aromaticity. However, as the system transitions from the gas phase to the solvent phase, the extent of this disruption decreases, as is evident from the data given in Tables 2 and 3.

Table 4. Contributions of TPB in gas, *n*-octanol, ethanol, and water media.

Atoms	HOMO				Atoms	LUMO			
	Gas	*n*-Octanol	Ethanol	Water		Gas	*n*-Octanol	Ethanol	Water
N3	6.02	6.23	6.28	6.30	N1	7.72	7.51	7.46	7.44
N4	6.02	6.23	6.28	6.30	N2	7.72	7.51	7.46	7.44
C11	7.96	7.49	7.32	7.24	C11	4.31	4.60	4.65	4.68
C12	8.91	8.41	8.24	8.16	C12	4.31	4.50	4.61	4.66
C13	8.91	8.41	8.24	8.16	C13	4.31	4.60	4.61	4.66
C14	7.96	7.49	7.32	7.24	C14	4.31	4.60	4.65	4.68
N33	8.22	8.35	8.46	8.50	C18	4.82	4.90	4.79	4.75
N35	4.00	4.22	4.25	4.27	C19	4.82	4.90	4.79	4.75
N37	4.00	4.22	4.25	4.27	C21	12.93	12.49	12.33	12.26
N39	8.22	8.36	8.46	8.51	C22	12.93	12.49	12.33	12.26
C41	8.29	8.60	8.71	8.76					
C43	8.29	8.60	8.71	8.76					

Table 5. HOMO, LUMO, and band gap energies of TPB.

Phase	E_{HOMO}	E_{LUMO}	ΔE_{gap}
Gas	-5.470721	-0.921862	4.548860
n-Octanol	-5.619304	-1.034047	4.585257
Ethanol	-5.655359	-1.053353	4.602005
Water	-5.673701	-1.064142	4.609560

(**a**) HOMO

(**b**) LUMO
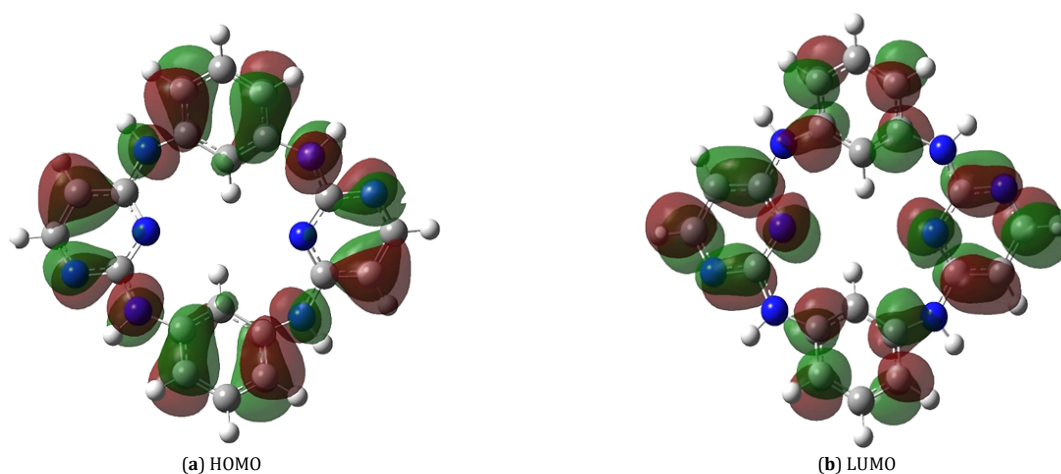
Figure 2. HOMO and LUMO for TPB.

The HOMO and LOMO schemes for in the gas phase for TPB are given in Figure 2. Atom contributions greater than 4% to HOMO and LUMO in gas, *n*-octanol, ethanol and water media are given in Table 4.

The contribution of atomic orbitals to HOMO expresses how much each atom in a molecule contributes to the electronic structure of HOMO, while the contribution to LUMO expresses how much each atom in a molecule contributes to the electronic structure of LUMO. HOMO is a high-energy molecular orbital filled with electrons and plays an important role in chemical reactions, ionization, and electronic transitions.

The contributions of N4 and C43 atoms from ring A, as well as N3 and C41 atoms from ring C, to the HOMO are equal, with values of 6.02 and 8.29, respectively. Similarly, the contributions of C12 and C14 from ring B, along with C11 and C13 from ring D, to the HOMO are also equal, with values of 7.96 and 8.91. The contributions of the N33, N37, N35 and N39 atoms from ring A to the HOMO are 4.00, 8.22, 4.00, and 8.22, respectively. The contributions of N3, N4, N33, N35, N39, C41, and C43 atoms in rings A and C to HOMO increased with the increase of the electric constant of the solvents, while the contributions of atoms (C11, C12, C13, C14) in rings B and D to HOMO decreased with the increase of the electric constant. The increase in the contributions of N3, N4, N33, N35, N37, N39, C41, and C43 atoms to the HOMO suggests that the mentioned atoms are more involved in the frontier molecular orbitals in polar solvents.

The contributions of N1, C21, and C18 atoms belonging to the A ring and N2, C22, and C19 atoms belonging to the C ring

to LUMO are the same, with values of 7.72, 12.93, and 4.82, respectively. The contributions of C12 and C14 atoms belonging to the B ring and C22 and C19 atoms belonging to the D ring to LUMO are identical and 4.31, 4.31. The contribution of N1, C21, N2 and C22 atoms belonging to the A and C rings to LUMO decreased with increasing dielectric constant of the solvent, in contrast, the contribution of C18 and C19, atoms belonging to the A and C rings to LUMO increased only in the *n*-octanol solvent. Electronic characteristics such as the HOMO energy (E_{HOMO}) and the LUMO energy (E_{LUMO}) and the TPB energy gap in the gas and *n*-octanol, ethanol, and water phases were analyzed using the DFT method with B3LYP/6-311G(d, p), level as listed in Table 5.

As seen in Table 5 the HOMO energy of the TPB molecule becomes more negative with the polarity of the phase. The E_{HOMO} of the TPB molecule shifts downward, and the shifting downward is the biggest (-5.673701) in the most polar solvent. The order of LUMO energy levels (from highest to lowest) of TPB is gas (-0.921862eV) > *n*-octanol (-1.034047 eV) > Ethanol (-1.053353eV) > water (-1.064142 eV) shows that LUMO energy becomes more negative) as the solvent polarity increases.

It is well known that the energy gap in the energy levels of a system, defined as $\Delta E_{gap} = E_{LUMO} - E_{HOMO}$, can indicate whether the molecule is hard or soft [25]. Hard molecules have a large HOMO-LUMO gap, while soft molecules have a small gap [25]. As shown in Table 5, the ΔE_{gap} in polar solvents is higher than in the gas phase.

Table 6. Summary of surface analysis for TPB in gas, *n*-octanol, ethanol, and water media.

The summary of surface analysis	Gas	*n*-Octanol	Ethanol	Water
V (Bohr^3)	2905.41	2905.94	2906.72	2907.07
OSA (Bohr^2)	1314.40	1313.45	1313.73	1313.78
PSA (Bohr^2)	555.18	557.20	558.79	559.10
NSA (Bohr^2)	759.22	756.24	754.94	754.69
OAV (kcal/mol)	-1.14	-2.08	-2.26	-2.36
PAV (kcal/mol)	12.69	14.51	14.72	14.84
NAV (kcal/mol)	-11.25	-14.30	-14.83	-15.10
OV ((kcal/mol)^2)	134.87	201.69	216.56	224.56
PV ((kcal/mol)^2)	77.92	104.11	107.91	109.77
NV ((kcal/mol)^2)	56.95	97.58	108.65	114.78
BC	0.24	0.25	0.25	0.25
PSM ((kcal/mol)^2)	32.90	50.37	54.14	56.11
ICS (kcal/mol)	11.71	14.14	14.52	14.72
G$_{min}$ (kcal/mol)	-36.20	-48.61	-51.43	-52.94
G$_{max}$ (kcal/mol)	42.39	49.08	49.95	50.34
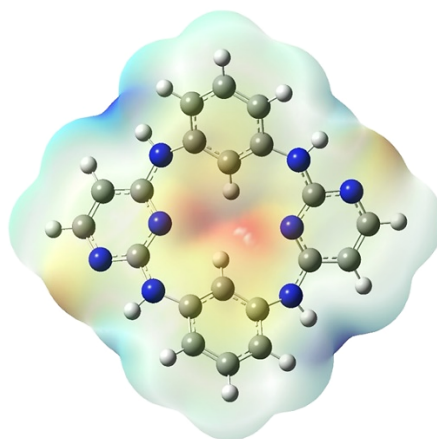
Figure 3. Electrostatic potential for TPB in gas phase red (very negative), yellow (slightly negative), light blue (positive), and dark blue (very positive).

The increase in the energy gap in polar solvents is due to the high chemical stability and low chemical reactivity of TPB in the solvents utilized [26]. The calculated 3D molecular electrostatic potential (MEP) surface of the TPB molecule performed from the optimized molecular structure at the B3LYP level and 6-311G(d,p) basis set in the gas phase, shown in Figure 3.

A molecular electrostatic potential map, which simultaneously displays the molecular size, shape, and electrostatic potential using color gradation, can be used to predict reactive sites for electrophilic and nucleophilic attacks. Blue indicates electron-deficient regions, green indicates nearly electrically neutral regions, and red indicates electron-rich regions.

Summary of surface analysis of TPB such as volume (V), overall surface area (OSA), positive surface area (PSA), negative surface area (NSA), overall average value (OAV), positive average value (PAV), negative average value (NAV), overall variance (OV), positive variance (PV), negative variance (NV), balance of charges (BC) product of σ_{tot}^2 and miu (PSM), and internal charge separation are given in Table 6.

The order of molecular volume (V) of TPB in different solvents: gas (2905.41 Bohr^3) < *n*-octanol (2905.94 Bohr^3) < ethanol (2906.72 Bohr^3) < Water (2907.07 Bohr^3). The molecular volume increases slightly as the polarity of the solvent increases. The smallest volume is in the gas phase, because there are no solvation effects.

The overall surface area and positive surface area slightly increase as the solvent polatiy increase. The OSA remains almost constant across different environments, indicating that solvent interactions do not significantly affect the total molecular surface. The molecular volume increases slightly from gas to water, suggesting minor expansion in polar solvents.

Therefore, the location and value of the ESP minimum on the molecular van der Waals (vdW) surface are often used to reveal the appropriate site of electrophilic attack [27]. The nucleophile carries a local positive charge and therefore tends to be attracted to the region where the ESP is positive. Therefore, the location and value of the ESP maxima on the molecular vdW surface are often used to reveal the appropriate site of nucleophilic attack [28].

Minimum 3 is the global minimum on the surface, and its large negative value is due to the lone pair of nitrogen, and the minimum energy value is -36.2041 kcal/mol. Maximum 2 is the global maximum arising from the positively charged H13 and the maximum energy value is 42.3938 kcal/mol.

The minimum energies for TPB in gas, *n*-octanol, ethanol, and water media are -36.20, 48.61, -51.43, and -52.94, respectively, indicating that the increase of the global minimum value of the dielectric constant increases as negative. Global maximum energies of TPB in gas, n-octanol, ethanol, and water media are 42.39, 49.08, 49.95, and 50.34 kcal/mol, respectively.

Figure 4 shows the relationship between the heat capacity, entropy, enthalpy and Gibbs free energy changes calculated using frequency calculations at temperatures ranging from 200 to 1000 K at the B3LYP/6-311G(d,p) level and the correlation equations and fittings fitted to the quadratic formula are depicted in Table 6 for the gas, *n*-octanol, ethanol and water phase.

Since the intensity of molecular vibrations increases with increasing temperature [29], thermodynamic properties such as heat capacity, entropy, enthalpy and Gibbs free energy changes also increase with temperature.

Previous reports have reported the effect of temperature variation on the thermodynamic properties of various drugs, including ferulic acid [30], ipriflavone [31], sinapic acid, and tinidazole [32].

Table 7. Equation for heat capacity (C), entropy (S), enthalpy (H), Gibbs free energy (G) of TPB.

Media	Equation *	R^2	Media	Equation *
Gas	$C = -0.0002 \times T^2 + 0.3906 \times T - 10.684$	0.9992	Ethanol	$C = -0.0002 \times T^2 + 0.3906 \times T - 10.4870$
	$S = 0.00005 \times T^2 + 0.3583 \times T + 57.418$	1		$S = 0.00005 \times T^2 + 0.3591 \times T + 56.5680$
	$H = 0.0001 \times T^2 + 0.0753 \times T - 10.453$	0.9997		$H = 0.0001 \times T^2 + 0.0753 \times T - 10.453$
	$G = -0.0002 \times T^2 - 0.1213 \times T + 7.0848$	1		$G = -0.0002 \times T^2 - 0.1213 \times T + 7.0848$
n-Octanol	$C = -0.0002 \times T^2 + 0.3906 \times T - 10.566$	0.9992	Water	$C = -0.0002 \times T^2 + 0.3906 \times T - 10.4900$
	$S = 0.00005 \times T^2 + 0.3588 \times T + 56.452$	1		$S = 0.00005 \times T^2 + 0.3591 \times T + 55.9770$
	$H = 0.0001 \times T^2 + 0.0753 \times T - 10.453$	0.9997		$H = 0.0001 \times T^2 + 0.0753 \times T - 10.4530$
	$G = -0.0002 \times T^2 - 0.1213 \times T + 7.0848$	1		$G = -0.0002 \times T^2 - 0.1213 \times T + 7.0848$

* Heat capacity (C), entropy (S), enthalpy (H), Gibbs free energy (G).

(a) Gas phase

(b) *n*-Octanol
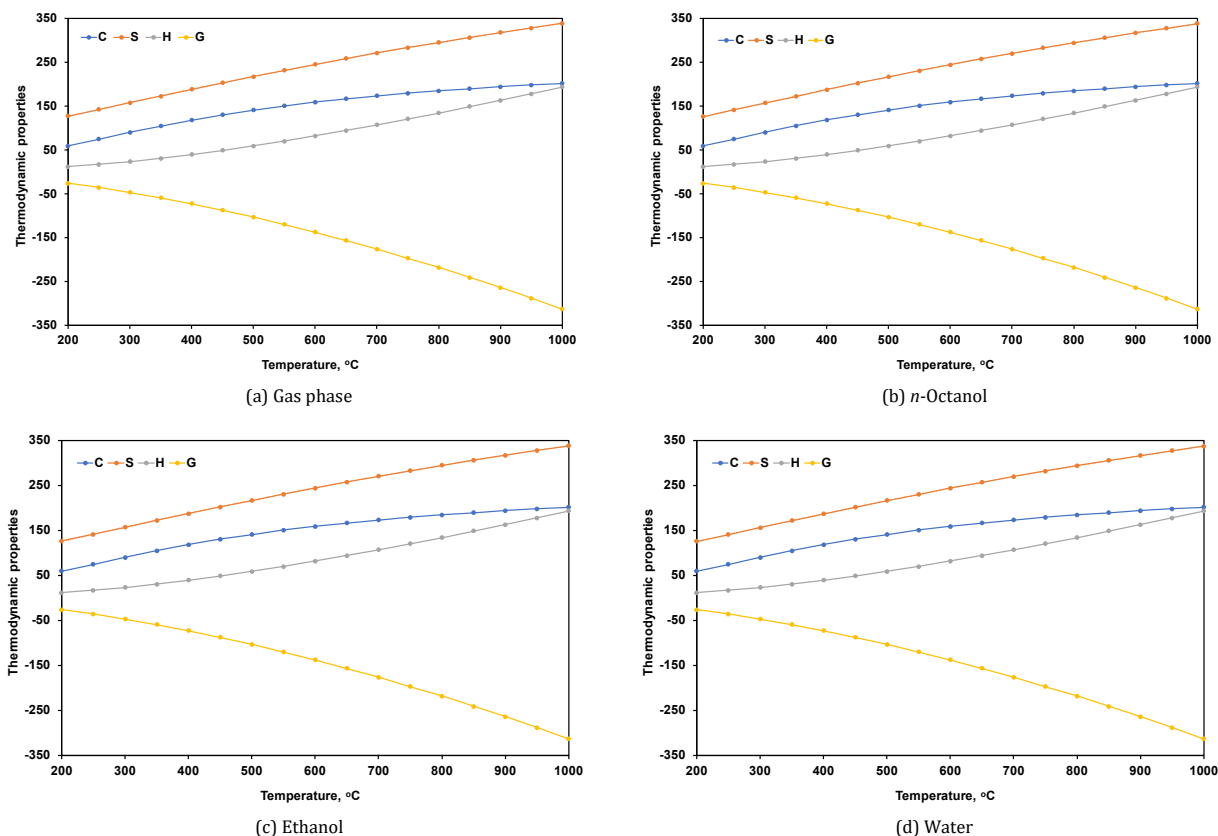
(c) Ethanol

(d) Water

Figure 4. The correlation graphs between various temperature versus Heat capacity (C), Entropy (S), Enthalpy (H), Gibbs free energy (G) of the title compound in (a) gas, (b) *n*-octanol, (c) ethanol, and (d) water phase.

The relationship between temperature and thermodynamic properties is modelled using a quadratic equation, yielding Table 7, which shows high correlation coefficients for the gas phase and solvent phases including n-octanol, ethanol, and water. These equations will be helpful for further studies of the title compound. The heat capacity in the octanol phase increased by 0.22082% at 200 K compared to the gas phase and by 0.03173% at 1000 K. Equations for heat capacity (C), entropy (S), enthalpy (H), Gibbs free energy (G) of TPB are given in Figure 4.

As seen in Table 7, the heat capacity equations for the gas and solvent phases are identical in their quadratic and linear terms, differing only slightly in their constants. Due to the negative quadratic term, the heat capacity in both phases decreases at very low temperatures. The entropy equation for the gas phase is $S = 0.00005 \times T^2 + 0.3583 \times T + 57.418$. In the equations for the solvent phase, the quadratic and linear terms are identical, the constant term is different. Because of the positive linear term, the entropy increases with temperature and because of small differences in the constant, there are slight differences in the gas, *n*-octanol, ethanol and water phases. Because Gibbs free energy decreases with increasing temperature due to the negative terms in the equation, this

means that, at high temperatures, the thermodynamic spontaneity of reactions involving these solvent increases.

4. Conclusions

In this study, quantum chemistry calculations are performed at the B3LYP/6 311G(d,p) level of theory to investigate the effect of the solvents studied on the stability order and aromaticity related to the HOMA index. The energies of the highest energy occupied molecular orbital (E_{HOMO}) and lowest energy unoccupied molecular orbital (E_{LUMO}) and energy gaps ΔE were also performed. Our theoretical results reveal that the energy gap and hardness of the studied complex increase with the increase in the dielectric constant of the solvent. This study comprehensively investigated the aromaticity, electronic structure, and surface properties of TPB in different solvent environments. The results show that the pyrimidine ring retains high aromaticity in all phases even with minimal distortions due to scriber interaction, while the benzene ring exhibits increased aromaticity in polar solvents. According to the HOMO-LUMO vacancy analysis, TPB exhibits greater stability and lower chemical reactivity in more polar solvents. The Molecular Electrostatic Potential (MEP) mapping

reveals that electrophilic and nucleophilic attack sites are affected by the solvent polarity. These findings contribute to a deeper understanding of the solvent-dependent electronic and structural behavior of TPB, which is critical for its application in chemical and biological systems. This study provides important chemical insights for pharmaceutical development, providing insight into the efficacy and stability of TPB under different solvent polarities and temperatures. In general, these equations show that gas, ethanol, *n*-octanol, and water behave similarly in terms of thermodynamic properties, with only minor changes.

Disclosure statement DS

Conflict of interest: The authors declare that they have no conflict of interest.
Ethical approval: All ethical guidelines have been adhered to.
Data availability: The data are available from the author.

CRediT authorship contribution statement CR

Conceptualization: Fatma Kandemirli; Methodology: Fatma Kandemirli; Software: Fatma Kandemirli, Alihan Tosun; Validation: Fatma Kandemirli, Alihan Tosun; Formal Analysis: Fatma Kandemirli, Alihan Tosun; Investigation: Fatma Kandemirli, Alihan Tosun Resources: Fatma Kandemirli, Alihan Tosun Data Curation: Fatma Kandemirli, Alihan Tosun Writing - Original Draft: Fatma Kandemirli; Writing - Review and Editing: Fatma Kandemirli, Alihan Tosun; Visualization: Fatma Kandemirli, Alihan Tosun; Supervision: Fatma Kandemirli; Project Administration: Fatma Kandemirli, Alihan Tosun.

ORCID iD and Email ✉

Alihan Tosun
✉ mioalihan27@gmail.com
iD https://orcid.org/0000-0002-8124-5442
Fatma Kandemirli
✉ fkandemirli@yahoo.com
iD https://orcid.org/0000-0001-6097-2184

References

[1]. Rashid, M.; Husain, A.; Shaharyar, M.; Mishra, R.; Hussain, A.; Afzal, O. Design and synthesis of pyrimidine molecules endowed with thiazolidin-4-one as new anticancer agents. *Eur. J. Med. Chem.* **2014**, *83*, 630–645.

[2]. Abdel-Mohsen, H. T.; Ragab, F. A.; Ramla, M. M.; El Diwani, H. I. Novel benzimidazole–pyrimidine conjugates as potent antitumor agents. *Eur. J. Med. Chem.* **2010**, *45* (6), 2336–2344.

[3]. Shruthi, N.; Poojary,B.; Kumar, V.; Bhat,M.; Joshi,H.; Revanasiddappa, B. C. Synthesis, molecular properties and evaluation of anthelmintic activity of new thiazolopyrimidine derivatives, *J. Chem. Pharm. Res.* **2015**, *7*, 181–191.

[4]. Mohan, N. R.; Sreenivasa, S.; Manojkumar, K. E.; Rao, T. M.; Thippeswamy, B. S.; Suchetan, P. A. Synthesis, Antibacterial, Anthelmintic and Anti-Inflammatory Studies of Novel Methylpyrimidine Sulfonyl Piperazine Derivatives. *J. Brazilian Chem. Soc.* **2014**, *25* (6), 1012-1020. https://doi.org/10.5935/0103-5053.20140073.

[5]. Abdel Moty, S. G.; Hussein, M. A.; Abdel Aziz, S. A.; Abou-Salim, M. A. Design and synthesis of some substituted thiazolo[3,2-a]pyrimidine derivatives of potential biological activities. *Saudi Pharmaceutical Journal* **2016**, *24* (2), 119–132.

[6]. Boschi, D.; Tosco, P.; Chandra, N.; Chaurasia, S.; Fruttero, R.; Griffin, R.; Wang, L.; Gasco, A. 6-Cyclohexylmethoxy-5-(cyano-NNO-azoxy)pyrimidine-4-amine: A new scaffold endowed with potent CDK2 inhibitory activity. *Eur. J. Med. Chem.* **2013**, *68*, 333–338.

[7]. Chan, S.; Han, K.; Qu, R.; Tong, L.; Li, Y.; Zhang, Z.; Cheng, H.; Lu, X.; Patterson, A.; Smaill, J.; Ren, X.; Ding, J.; Xie, H.; Ding, K. 2,4-Diarylamino-pyrimidines as kinase inhibitors co-targeting IGF1R and EGFRL858R/T790M. *Bioorganic & Medicinal Chemistry Letters* **2015**, *25* (19), 4277–4281.

[8]. Addepalli, Y.; Yang, X.; Zhou, M.; Reddy, D. P.; Zhang, S.; Wang, Z.; He, Y. Synthesis and anticancer activity evaluation of novel azacalix[2]arene[2]pyrimidines. *Eur. J. Med. Chem.* **2018**, *151*, 214–225.

[9]. Siegel, R. L.; Miller, K. D.; Jemal, A. Cancer statistics, 2016. *CA. A. Cancer J. Clinicians* **2016**, *66* (1), 7–30.

[10]. Vineis, P.; Wild, C. P. Global Cancer Patterns: Causes and Prevention. *Lancet* **2014**, *383* (9916), 549–557.

[11]. Chtita, S. Modélisation de molécules organiques hétérocycliques biologiquement actives par des méthodes QSAR/QSPR. Recherche de nouveaux médicaments. Doctoral Dissertation, Université Moulay Ismaïl, Meknès, 2017. https://hal.science/tel-01568788v1

[12]. Levine I. N. Quantum Chemistry Chemistry Semiempirical and Molecular-Mechanics Treatments of Molecules Department, Brooklyn College, City University of New York.

[13]. Becke, A. D. Density-functional thermochemistry. III. The role of exact exchange. *The Journal of Chemical Physics* **1993**, *98* (7), 5648–5652.

[14]. Frisch, M. J.; Trucks, G. W.; Schlegel, H. B.; Scuseria, G. E.; Robb, M. A.; Cheeseman, J. R.; Montgomery, J. A.; Vreven, T.; Kudin, K. N.; Burant, J. C.; Millam, J. M.; Iyengar, S. S.; Tomasi, J.; Barone, V.; Mennucci, B.; Cossi, M.; Scalmani, G.; Rega, N.; Petersson, G. A.; Nakatsuji, H.; Hada, M.; Ehara, M.; Toyota, K.; Fukuda, R.; Hasegawa, J.; Ishida, M.; Nakajima, T.; Honda, Y.; Kitao, O.; Nakai, H.; Klene, M.; Li, X.; Knox, J. E.; Hratchian, H. P.; Cross, J. B.; Adamo, C.; Jaramillo, J.; Gomperts, R.; Stratmann, R. E.; Yazyev, O.; Austin, A. J.; Cammi, R.; Pomelli, C.; Ochterski, J. W.; Ayala, P. Y.; Morokuma, K.; Voth, G. A.; Salvador, P.; Dannenberg, J. J.; Zakrzewski, V. G.; Dapprich, S.; Daniels, A. D.; Strain, M. C.; Farkas, O.; Malick, D. K.; Rabuck, A. D.; Raghavachari, K.; Foresman, J. B.; Ortiz, J. V.; Cui, Q.; Baboul, A. G.; Clifford, S.; Cioslowski, J.; Stefanov, B. B.; Liu, G.; Liashenko, A.; Piskorz, P.; Komaromi, I.; Martin, R. L.; Fox, D. J.; Keith, T.; Al-Laham, M. A.; Peng, C. Y.; Nanayakkara, A.; Challacombe, M.; Gill, P. M. W.; Johnson, B.; Chen, W.; Wong, M. W.; Gonzalez, C.; Pople, J. A. Gaussian, Inc., Wallingford CT, 2004.

[15]. Dennington, R.; Keith, T. A.; Millam, J. M. GaussView, Version 6, Semichem Inc.; Shawnee Mission, KS, 2016.

[16]. Cancès, E.; Mennucci, B.; Tomasi, J. A New Integral Equation Formalism for the Polarizable Continuum Model: Theoretical Background and Applications to Isotropic and Anisotropic Dielectrics. *J. Chem. Phys.* **1997**, *107* (8), 3032–3041.

[17]. Bharathy, G.; Christian Prasana, J.; Muthu, S.; Irfan, A.; Basha Asif, F.; Saral, A.; Aayisha, S.; Niranjana devi, R. Evaluation of electronic and biological interactions between N-[4-(Ethylsulfamoyl)phenyl] acetamide and some polar liquids (IEFPCM solvation model) with Fukui function and molecular docking analysis. *J. Molecular Liquids* **2021**, *340*, 117271.

[18]. Selvakumari, S.; Murthy Potla, K.; Shanthi, D.; Irfan, A.; Muthu, S. Solvent effect on molecular, electronic parameters, topological analysis and Fukui function evaluation with biological studies of imidazo [1, 2-a] pyridine-8-carboxylic acid. *J. Molecular Liquids* **2023**, *382*, 121863.

[19]. Lee, C.; Yang, W.; Parr, R. G. Development of the Colle-Salvetti correlation-energy formula into a functional of the electron density. *Phys. Rev. B.* **1988**, *37* (2), 785–789.

[20]. Lu, T.; Chen, F. -W. Calculation of Molecular Orbital Composition[J]. *Acta Chimica Sinica*, **2011**, *69*(20): 2393–2406. https://sioc-journal.cn/Jwk_hxxb/EN/abstract/abstract340458.shtml

[21]. Lu, T.; Chen, F. Quantitative Analysis of Molecular Surface Based on Improved Marching Tetrahedra Algorithm. *J. Mol. Graph. Model.* **2012**, *38*, 314–323.

[22]. Pedersen, J.; Mikkelsen, K. V. A benchmark study of aromaticity indexes for benzene, pyridine and the diazines – I. Ground state aromaticity. *RSC. Adv.* **2022**, *12* (5), 2830–2842.

[23]. Gajda, L.; Kupka, T.; Broda, M. A. Solvent impact on the planarity and aromaticity of free and monohydrated zinc phthalocyanine: a theoretical study. *Struct. Chem.* **2017**, *29* (3), 667–679.

[24]. Lu, T.; Chen, F. Multiwfn: A multifunctional wavefunction analyzer. *J. Comput. Chem.* **2011**, *33* (5), 580–592.

[25]. Parr, R. G.; Pearson, R. G. Absolute Hardness: Companion Parameter to Absolute Electronegativity. *J. Am. Chem. Soc.* **1983**, *105* (26), 7512–7516.

[26]. Omer, R.; Ahmed, L.; Qader, I.; Koparir, P. Theoretical Analysis of the Reactivity of Carmustine and Lomustine Drugs. *Journal of Physical Chemistry and Functional Materials* **2022**, *5* (1), 84–96.

[27]. Scrocco, E.; Tomasi, J. The Electrostatic Molecular Potential as a Tool for the Interpretation of Molecular Properties. In Topics in Current Chemistry Fortschritte der Chemischen Forschung; Springer Berlin Heidelberg: Berlin, Heidelberg, 2007; pp 95–170.

[28]. Gadre, S. R.; Suresh, C. H.; Mohan, N. Electrostatic potential topology for probing molecular structure, bonding and reactivity. *Molecules* **2021**, *26*, 3289.

[29]. Tanış, E.; Babur Sas, E.; Kurban, M.; Kurt, M. The structural, electronic and spectroscopic properties of 4FPBAPE molecule: Experimental and theoretical study. *J. Mol. Struc.* **2018**, *1154*, 301–318.

[30]. Sherefedin, U.; Belay, A.; Gudishe, K.; Kebede, A.; Kumela, A. G.; Wakjira, T. L.; Asemare, S.; Gurumurthi, T. Effects of temperature and solvent polarity on the thermodynamic and photophysical properties of ferulic acid using density functional theory (DFT). *Journal of Molecular Liquids* **2024**, *407*, 125175.

[31]. Huang, Z.; Zun, Y.; Gong, Y.; Hu, X.; Sha, J.; Li, Y.; Li, T.; Ren, B. Solid-Liquid Equilibrium Solubility, Thermodynamic Properties, Solvent

Effect of Ipriflavone in Twelve Pure Solvents at Various Temperatures. *J. Chem. Thermodyn.* **2020**, *150* (106231), 106231.

[32]. Li, T.; Zhu, L.; Li, J.; Cao, Z.; Sha, J.; Li, Y.; Ren, B. Solubility, thermodynamic properties and molecular simulation of tinidazole in fourteen mono-solvents at different temperatures. *The Journal of Chemical Thermodynamics* **2022**, *170*, 106767.